EPJ Web of Conferences **181**, 01032 (2018) https://doi.org/10.1051/epjconf/201818101032
*EXA2017*

# Low-energy electron-positron collider to search and study ($\mu^+\mu^-$) bound state

*Anton Bogomyagkov*[*], *Vladimir Druzhinin*, *Eugene Levichev*, *Alexander Milstein*, and *Sergej Sinyatkin*

*Budker Institute for Nuclear Physics, Novosibirsk 630090, Russia*

**Abstract.** We discuss a low energy $e^+e^-$ collider for production of the not yet observed ($\mu^+\mu^-$) bound system (dimuonium). Collider with large crossing angle for $e^+e^-$ beams intersection produces dimuonium with non-zero momentum; therefore, its decay point is shifted from the beam collision area providing effective suppression of the elastic $e^+e^-$ scattering background. The experimental constraints define subsequent collider specifications. We show preliminary layout of the accelerator and obtained main parameters. High luminosity in chosen beam energy range allows to study $\pi^\pm$ and $\eta$-mesons.

## 1 Introduction

Currently some authors consider a lepton atom ($\mu^+\mu^-$)[a] as a strong candidate for casting light on disagreement between the anomalous magnetic moment measurement and Standard Model prediction, the muonic hydrogen proton's charge radius discrepancy, etc. [2, 3]. Even if this expectation will not come true, a discovery of a new lepton bound state, which has not been observed yet contrary to positronium ($e^+e^-$) and muonium ($\mu^+e^-$), and its study is by far a challenging and interesting scientific enterprise. Like positronium, dimuonium is a Bohr atom and its study (including transition spectroscopy, lifetime precise measurement, etc.) allows verifying QED and quantum mechanics computations with great accuracy. In such a research, ($\mu^+\mu^-$) has higher new-physics reach potential in comparison with other exotic atoms. It has larger reduced mass $\mu = m_\mu/2$ than ($e^+e^-$) and ($\mu^+e^-$), for which $\mu \approx m_e$; therefore, it is considerably more compact (the dimuonium Bohr radius is 200 times smaller than the positronium one). In contrast to ($pe^-$) and ($p\mu^-$) systems, ($\mu^+\mu^-$) experiences no strong interaction obscuring exploration of tiny QED effects. Study of heavier and more compact taonium ($\tau^+\tau^-$) would also be interesting but its production is extremely difficult even if compared with ($\mu^+\mu^-$).

In the past, many of proposed ($\mu^+\mu^-$) production channels have been discussed [1, 4-13] including those from electron and positron collision [1, 5, 10]. The $e^+e^-\rightarrow$ ($\mu^+\mu^-$) production mechanism is particularly interesting because it contains no hadrons which, otherwise, should be untangled in the reconstruction process. However, a $e^+e^-$ collider for the dimuonium experimental study has never been discussed in details.

We propose a preliminary design of the electron-positron collider for ($\mu^+\mu^-$) search and study. Low beam energy $E_b \approx 400$ MeV results in a compact machine, inexpensive in both manufacture and maintenance. Large crossing angle of the intersecting beams induces a non-zero dimuonium momentum, which is a distinct feature of our design (originally proposed in [10]). In this case, the ($\mu^+\mu^-$) production and decay points are separated along the beams directions bisector (for equal beam energies). The distance between the atom formation and its annihilation into $e^+e^-$ pair effectively suppresses elastic scattering background from the primary beams and allows unambiguous detection of dimuonium decay.

The collider design is rather challenging, because large collision is a source of various effects in $e^+e^-$ beams interaction, absent in the head-on collisions. Low beam energy and high bunch intensity result in the strong intra-beam scattering (IBS) and reduced Touschek lifetime. We discuss and estimate all these issues below.

Besides the ($\mu^+\mu^-$) research, the beam energy and collider configuration allow studying such processes as $e^+e^-\rightarrow$ *pions* and $e^+e^-\rightarrow \eta,\eta'$ substantially expanding experimental program of the facility.

## 2 Dimuonium

We briefly present the major properties of ($\mu^+\mu^-$) atom relevant to the collider design. More detailed information can be found elsewhere (see for instance [14] and references therein).

Dimuonium is one of the simplest hydrogen-like atoms and its spectrum in the first approximation is similar to the positronium spectrum with respectful mass substitution. Unlike positronium, dimuonium annihilates into $e^+e^-$ pair, which makes its formation and spectrum more sensitive to vacuum polarization effects caused by

[a] Dubbed "dimuonium", "bimuonium" or "true muonium".

[*] Corresponding author: author@e-mail.org

virtual electron-positron pairs production. Fig.1 shows dimuonium energy levels.

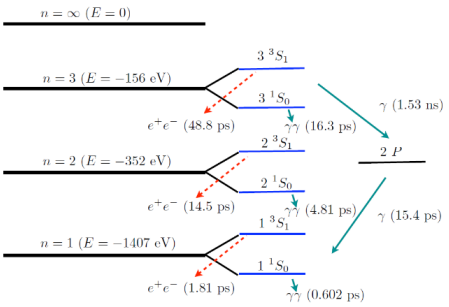


**Fig. 1.** The dimuonium energy states diagram [10] (not in scale).

Dimuonium Bohr radius is $R_{\mu\mu} = 512$ fm (for reference the positronium Bohr radius is $R_{ee} = 0.106$ nm). The ($\mu^+\mu^-$) atom exists in two spin states: paradimuonium, which is a singlet with total muon-antimuon spin S = 0, and orthodimuonium (triplet S = 1). For paradimuonium ground state with the dominant decay mode $1^1S_0 \rightarrow \gamma\gamma$ the lifetime is 0.602 ps while for orthodimuonium it is of 1.81 ps (dominant decay is $1^3S_1 \rightarrow e^+e^-$). Muon weak decay is very slow with the lifetime of 2.2 μs, and thus, dimuonium is a unique metastable system available for precision QED tests.

Cross section of ($\mu^+\mu^-$) production in the electron-positron collision for exact resonance condition (the beam energy $E_b = m_\mu - \Delta_{\mu\mu}/2$, $m_\mu$ is the muon mass and $\Delta_{\mu\mu} \approx 1.41$ keV is the binding energy) is [1]

$$\sigma_{\mu\mu n} = 3.3 \cdot 10^{-25} n^{-3} \text{ cm}^2 \quad (1)$$

The cross section (1) rapidly decreases with the principal quantum number $n$. Radiative corrections reduce the cross section, the ground state reduction is [1]

$$\sigma_{\mu\mu 1R} = 0.27\sigma_{\mu\mu 1}. \quad (2)$$

However, detailed simulation of the ($\mu^+\mu^-$) production rate with account for the beam energy and spatial distribution [16] recovers the cross section reduction due to the radiative corrections (within 10% accuracy), thus for convenience to estimate the dimuonium production rate below we use the cross section (1).

## 3 Large angle beam crossing

To study the beams collision with an arbitrary angle we apply results from [15]. Two leptons with four-momenta $(E_1, \boldsymbol{p}_1)$ and $(E_2, \boldsymbol{p}_2)$ collide as shown in Fig.2.

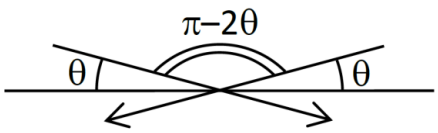


**Fig. 2.** Electron positron ccollision at arbitrary angle θ.

Head-on collision corresponds to $\theta = 0$ and parallel momenta at $\theta = \pi/2$. Assuming Gaussian beam energy spread with r.m.s. $\sigma_\delta = \sigma_E/E_0$ and where $E_0$ is beam average energy, Gaussian angular spreads in horizontal and vertical planes with r.m.s. $\sigma_{x'}$ and $\sigma_{y'}$ we obtain invariant mass mean and r.m.s. values

$$\langle M\rangle_{x',y',\delta} = 2E_0\cos\theta - \frac{E_0}{2}\left(\sigma_\delta^2\cos\theta - \sigma_{x'}^2\cos\theta - \sigma_{y'}^2\frac{\cos 2\theta}{\cos\theta}\right), \quad (3)$$

$$\sigma_M^2 = 2E_0^2(\sigma_\delta^2\cos^2\theta + \sigma_{x'}^2\sin^2\theta). \quad (4)$$

For short bunches (a *hour-glass* effect is neglected) with equal population $N$, colliding with the frequency $f_0$ at the arbitrary angle $\theta$ the peak luminosity is

$$L_0 = \frac{N^2}{4\pi\sigma_x\sigma_y\sqrt{1+\varphi^2}}f_0, \quad (5)$$

where $\sigma_{x,y}$ is transverse r.m.s. beam size at the interaction point (IP), $\varphi = \sigma_z\tan\theta/\sigma_x$ is Piwinski angle, $\sigma_z$ is bunch length. For large Piwinski angle $\varphi \gg 1$ and the peak luminosity

$$L_0 \approx \frac{N^2}{4\pi\sigma_y\sigma_z\tan\theta}f_0 \quad (6)$$

is less than head-on luminosity and does not depend on the horizontal beam size at IP.

Using approximate expression for ($\mu^+\mu^-$) production cross section

$$\sigma(x'_{1,2}, y'_{1,2}, \delta_{1,2}) = \Gamma_{\mu\mu}\sigma_{\mu\mu}\delta\left(M(x'_{1,2}, y'_{1,2}, \delta_{1,2}) - m_{\mu\mu}\right), \quad (7)$$

we calculated dimuonium production rate as convolution of cross section with differential luminosity ([15])

$$\dot{N}_{\mu\mu} = \frac{L_0\Gamma_{\mu\mu}\sigma_{\mu\mu}}{2\sqrt{\pi}\sigma_M}. \quad (8)$$

Non-zero $e^+e^-$ crossing angle boosts the atom to move along the bisector of the beam lines (for equal $e^+e^-$ energies); therefore, with given dimuonium lifetime at rest $\tau_{0\mu\mu} = \hbar/\Gamma_{\mu\mu}$, the annihilation point is separated from the formation point by

$$l = c\,\tau_{0\mu\mu}\beta_{\mu\mu}\gamma_{\mu\mu} = c\,\tau_{0\mu\mu}\tan\theta = \frac{c\hbar}{\Gamma_{\mu\mu}}\tan\theta, \quad (9)$$

where $c$ is speed of light, $\beta_{\mu\mu}$ and $\gamma_{\mu\mu}$ are dimuonium normalized velocity and Lorentz factor.

## 4 Beam-beam effects

Contrary to the head-on collision, the opposite bunch forces in the large crossing angle collision are not purely transverse, and depend on longitudinal coordinates of the suffering particle. Authors of [17, 18, 19] considered beam-beam effects for arbitrary crossing angle and showed that transverse influence is suppressed, but longitudinal is emphasized for large angles. The beam-beam tune shifts for flat beams ($\sigma_y \ll \sigma_x$) clearly illustrate this fact:

$$\xi_y = \frac{Nr_e}{2\pi\gamma}\frac{\beta_y}{\sigma_y\sqrt{\sigma_x^2 + \sigma_z^2\tan^2\theta}}, \quad (10)$$

$$\xi_x = \frac{Nr_e}{2\pi\gamma}\frac{\beta_x}{\sigma_x^2 + \sigma_z^2\tan^2\theta}, \quad (11)$$

where $\beta_{x,y}$ are betatron functions at IP, $r_e$ is classical electron radius, and

$$\xi_z = -\frac{N r_e}{2\pi\gamma}\frac{\sigma_{z0}\tan^2\theta}{\sigma_{\delta 0}(\sigma_x^2+\sigma_{z0}^2\tan^2\theta)}\frac{\alpha}{|\alpha|}, \qquad (12)$$

where $\sigma_{\delta 0}$ and $\sigma_{z0}$ are the energy spread and bunch length of the "strong" beam affecting the test particle (weak-strong approximation). Bunch population $N$, Lorentz factor $\gamma$, and IP beam sizes $\sigma_x$ and $\sigma_z$ also belong to the "strong" bunch.

For some (not necessary large) intersection angle $\theta$ we have $\sigma_z\tan\theta \gg \sigma_z$, and the conventional transverse beam-beam effects (10) (11) are suppressed. Longitudinal beam-beam effects (12) increase, and the synchrotron tune shift

$$\Delta\nu_s = \xi_z \approx -\frac{N r_e}{2\pi\gamma}\frac{1}{\sigma_{\delta 0}\sigma_{z0}}\frac{\alpha}{|\alpha|} \qquad (13)$$

might be as large as the unperturbed synchrotron tune $\nu_s$, causing the phase instability of the test bunch. Even below this limit, when the particle motion is still stable, the "strong" bunch electric field distorts RF bucket, modifies longitudinal bunch distribution, and reduces luminosity.

In canonical coordinates $(z, p_z)$, where $z$ is particle position with respect to the bunch center and $p_z$ is conjugate momentum, the linear Hamiltonian of the test particle longitudinal motion is

$$H_z \approx -\frac{\alpha\, p_z^2}{2} - \frac{\nu_s^2}{\alpha R^2}\frac{z^2}{2} - \frac{2\xi_z\nu_s}{\alpha R^2}\frac{z^2}{2}. \qquad (14)$$

The second term relates to accelerating RF system, the third one corresponds to the colliding bunch electrical field, α is momentum compaction factor, and $R$ is orbit average radius. To keep the bunch field effect negligible one needs $\xi_z \ll \nu_s/2$, which means either large synchrotron tune $\nu_s$ or small longitudinal beam-beam parameter (13) and finally limits the "strong" bunch population according to

$$N < \frac{2\pi R\,\gamma}{r_e}\frac{\alpha\,\sigma_\delta^2}{2}. \qquad (15)$$

This limit within the factor of two corresponds to the condition for coherent instability of two bunches intersecting at large angle found in [18].

From the Hamiltonian (14) one can see another possibility to suppress the longitudinal beam-beam effects. For positive momentum compaction $\alpha > 0$ the beam-beam synchrotron tune shift $\xi_z < 0$, and the "strong" bunch field flattens RF potential well, increases "weak" bunch length, and destroys stability. Alternatively, for magnetic lattice with $\alpha < 0$ the third term in (14) has the same sign as a second one, giving deeper RF potential well and smaller "weak" bunch length.

High order expansion of the synchrotron motion Hamiltonian shows that for $\alpha > 0$ the "strong" bunch field modulates RF potential well and splits the "weak" bunch into sub-bunches. Simulation with the help of the beam-beam computer code LIFETRAC [20] confirmed this effect as well as above estimation of the bunch intensity limit.

## 5 Background and choice of collider parameters

The main source of the background is elastic (Bhabha) $e^+e^- \to e^+e^-$ scattering with cross section $\sigma_{Bhabha} = 22000$ nb for crossing angles from 45° to 135°. For different collision schemes production cross section of $1^3S_1$ dimuonium state is $\sigma_{\mu\mu}(m_{\mu\mu}) = 0.23 \div 11$ nb. Background to signal ratio is than $(3 \div 130)\times 10^3$. Crossing angle collisions is the only way to suppress background, it separates dimuonium decay point from the origin point. For estimation of the signal to background ratio $\dot{N}_{\mu\mu}/\dot{N}_{ee}$, where $\dot{N}_{ee}$ is elastic scattering rate we use collision scheme shown on Fig. 3.

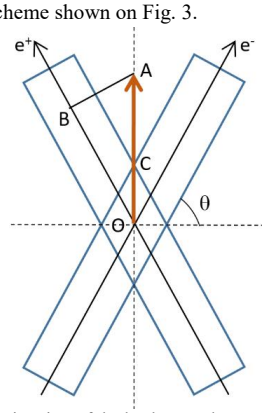


**Fig. 3.** On estimation of the background rate.

Points O and A are those of dimuonium production and decay; the distance $OA = l$ is defined in (9). At the point A, where $e^+e^-$ scattering mimics dimuonium decay, the density of the primary particles (assuming normal distribution) drops according to $N_1 = N_0\exp(-n_x^2/2)$, where $n_x = AB/\sigma_x$, $AB = l\cos\theta = c\,\tau_{0\mu\mu}\sin\theta$, and background rate $\dot{N}_{ee} \propto N_1^2$. Using $\sigma_M$ from (4) and substituting beam size and divergence with $\sigma_{x'}^2 = \varepsilon_x/\beta_x$ and $\sigma_x^2 = \varepsilon_x\beta_x$, $\varepsilon_x$ is horizontal emittance, we obtain signal to background ration estimation

$$\frac{\dot{N}_{\mu\mu}}{\dot{N}_e} \propto \frac{\exp\left(\frac{\left(c\,\tau_{0\mu\mu}\right)^2\sin^2\theta}{\sigma_x^2}\right)}{\sqrt{\sigma_\delta^2\cos^2\theta + (\sigma_x^2/\beta_x^2)\sin^2\theta}}. \qquad (16)$$

To increase numerator in (16) one needs the large crossing angle $\sin\theta \to 1$ ($\theta \to 90°$) and small horizontal beam size $\sigma_x^2 = \varepsilon_x\beta_x$ at the IP. To reduce denominator (better resolution) one needs small beam divergence $\sigma_{x'}^2 = \varepsilon_x/\beta_x$ at the IP. Large intersection angle increases required beam energy (3), enlarges the energy resolution (4), and strongly degrades the peak luminosity (5). The choice of collider parameters requires careful balance of pros and cons. Another important issue is existing injection facility [21] with capacity $(0.5 \div 1)\times 10^{10}\ e^+/s$ in the energy range of $E_{inj} \approx 350 \div 450$ MeV. Top-up injection (at the energy of experiment) allows reaching average luminosity close to the peak one. Despite the luminosity drop with the crossing angle increase, reduction of the beam interaction length permits decrease of the vertical beta $\beta_y$

at the IP (like for Crab-Waist collision [22]), this partially recovers the luminosity loss. In addition, the beam energy enlargement suppresses intra-beam scattering (IBS) and results in the collider performance enhancement.

The major specifications of the electron-positron collider for dimuonium production and exploration are:

1. The crossing angle of 75° allows ($\mu^+\mu^-$) production for the beam energy of $E_b$ = 408 MeV ($m_\mu$ = 105.7 MeV). At 70° $\pi^+\pi^-$ ($m_{\pi^\pm}$ = 139.6 МэВ) can be generated at the same beam energy. The angle modification is available either by mechanical rearrangement of the interaction area or using corrector magnets.
2. The crossing angle of 75° provides $1^3S_1$ ($\mu^+\mu^-$) decay path $l$ = 2 mm, it is enough to detect the atom decay to $e^+e^-$. For the next dimuonium terms, the lifetime (and the escape length) increases as $n^3$ (see Fig.1), however production rate falls down insofar.
3. To increase the signal-background ratio (16) the horizontal beam size at the IP should be $\sigma_x \ll c\,\tau_{0\,\mu\mu} = 0.54$ mm, so we take $\sigma_x < 0.15$ mm.
4. For large crossing angle, horizontal angular spread at the IP is the main source of the invariant mass resolution degradation. To reduce the angular spread with the small beam size collider has to provide low horizontal emittance.
5. Lattice with negative momentum compaction $\alpha < 0$ have been studied at several colliders (for instance, at KEKB [23] or at DAΦNE [24]). This operation mode has never been used as regular one. The explanation is that in such a mode microwave instability current threshold reduces, giving larger beam energy spread and transverse size (especially in vertical direction) and smaller luminosity [24]. Therefore, in our design we adopt a conservative but robust solution with positive α. Another argument in favor of $\alpha > 0$ is that the negative compaction lattice requires extra space for matching sections and the orbit length increases.
6. For high luminosity one needs highly populated $e^+e^-$ bunches but the longitudinal beam-beam effects limit the bunch intensity according to (15). In our specifications we take the bunch population $N_0 \le 3.5 \times 10^{10}$ $e^+/e^-$. To arrange a multi-bunch operation two separate storage rings are necessary.
7. Low vertical beta-function at the IP benefits to the high luminosity. However, extremely low beta causes strong chromatic effect in the final focus quadrupoles, which needs to be compensated by specially arranged chromatic correction sections. To reduce collider size we choose $\beta_y$ = 2 mm and avoid final focus local chromaticity correction.
8. Reverse of the beam circulation direction in one of the rings changes the crossing angle to 15°, and makes it possible to study with high luminosity energy range from η-meson ($m_\eta$ = 547.8 MeV, $E_b \approx$ 284 MeV at $\theta$ = 15°) to η′-meson ($m_{\eta'}$ = 957.7 MeV, $E_b \approx$ 496 MeV).

## 6 Collider

A simple and symmetric configuration of the large crossing angle collider consists of two identical bulb-shape storage rings with two intersection points. Fig. 4 shows $e^+e^-$ orbits for such configuration. Each ring includes two straight interaction sections and two closing arcs: inward and outward. The collider footprint is 12×6 м$^2$, and the ring circumference is about 23 m.

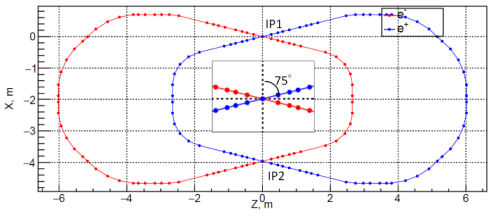


**Fig. 4.** Orbits of $e^+e^-$ collider rings.

Fig. 5 presents the magnet sequence and the lattice functions along the ring. The inward arc lattice (IP1-IP2) is a Double Bend Achromat (DBA) with the IP betatron functions $\beta_y$ = 2 mm and $\beta_x$ = 20 cm. The maximum vertical beta in the first defocusing final focus quadrupole is not large ($\beta_y \approx$ 50 m) and the local chromatic section is unnecessary. The outward Multipole Bend Achromat (MBA) arc (IP2-IP1) provides low radiative emittance [25]. Table 1 gives the main parameters of the ring at 408 MeV.

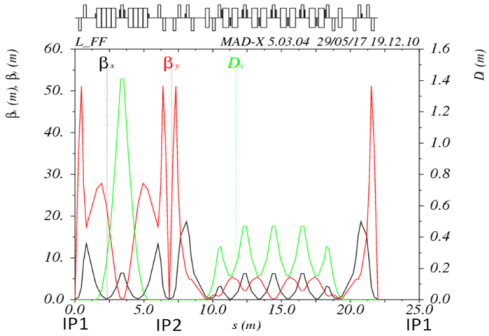


**Fig. 5.** Lattice functions of the storage ring.

The momentum compaction factor is quite large $\alpha$ = 0.064, so condition $\xi_z \ll \nu_s/2$ is well satisfied. The longitudinal beam-beam effects define the maximum bunch intensity (15) as $N_{max} = 1.5 \times 10^{11}$. We have chosen $N = 3.5 \times 10^{10}$ and it is rather adequate for reliable operation. The transverse beam-beam effects are negligible; therefore, other reasons define the choice of the betatron tune point (for instance, size of dynamic aperture or momentum acceptance). The lattice provides radiative emittance of $\varepsilon_x$ = 26 nm, which IBS increases by factor of four. IBS elongates the bunch length from natural 5.4 mm to 11.6 mm. Touschek beam lifetime for the pa-rameters given in Table 1 is around 1500 s.

The primary $e^+e^-$ collisions beyond the point A in Fig.3 determine elastic scattering background rate.

**Table 1.** Collider main parameters at 408 MeV.

| | |
|---|---|
| Beam energy (MeV) | 408 |
| Circumference (m) | 23 |
| Bunch intensity/current (mA) | $3.5\times10^{10}$/73 |
| Revolution frequency/period (MHz)/(ns) | 13.04/76.7 |
| RF harmonic number/frequency (MHz) | 26/338.98 |
| Energy loss per turn (keV) | 2.3 |
| RF voltage (kV) | 450 |
| RF acceptance | 2% |
| Synchrotron tune | $1.71\times10^{-2}$ |
| Momentum compaction $\alpha$ | $6.4\times10^{-2}$ |
| Damping time hor/ver/long (ms) | 17.3/27.3/22.1 |
| Damping partition hor/long | 1.6/1.4 |
| Horizontal emittance (without/with IBS) (nm) | 26/90 |
| Energy spread (without/with IBS), $\times10^4$ | 4/8.4 |
| Bunch length (without/with IBS) (mm) | 5.4/11.6 |
| Betatron coupling | 0.3% |
| IP horizontal angular spread $\sigma_{x\prime} \times 10^4$ | 6.7 |
| Invariant mass resolution (keV) | 390 |
| Hor/vert betatron function at IP (mm) | 200/2 |
| Hor/vert betatron size at IP (μm) | 130/0.7 |
| Hor/vert beam-beam parameter ($\xi_x/\xi_y$) | $2\times10^{-6}/1.2\times10^{-3}$ |
| Longitudinal beam-beam parameter $\xi_z$ | $-2\times10^{-3}$ |
| Peak luminosity for 1 bunch ($cm^{-2}s^{-1}$) | $4\times10^{30}$ |
| Peak luminosity for 20 bunches ($cm^{-2}s^{-1}$) | $8\times10^{31}$ |

Assuming Gaussian distribution of the beam particles along the dimuonium escape line with standard deviation $OC = \sigma_x/\cos\theta$, the number of the electrons in the beam tail beyond the A divided by the total amount of beam electrons is

$$\frac{N_{>A}}{N_\Sigma} \propto 1 - \mathrm{erf}\left(\frac{OA}{\sqrt{2}\,OC}\right) = 1 - \mathrm{erf}\left(\frac{l\,\cos\theta}{\sqrt{2}\,\sigma_x}\right). \quad (17)$$

Our parameters provide $OA > 2$ mm and suppress the particle density in the beam tail (and the elastic scattering background rate) by 4.5 standard deviations for the ground state $1^3S_1$.

There are eight bending magnets in each ring. Two magnets compose the DBA cell of the inward arc. Six magnets compose the regular MBA cell in the outward arc and two additional magnets cancel dispersion function in the interaction region. All bending magnets have the same magnetic field (1.27 T at 408 MeV) and low negative gradient to reduce the number of defocusing quadrupoles, to increase horizontal partition number and to reach smaller emittance. The regular magnets in the MBA cell are split into two halves with defocusing sextupoles installed in between, at the azimuth with the best ratio of the vertical-to-horizontal betas. Twenty quadrupoles combined in 10 families determine the ring optical functions. The maximum gradient in the arc quadrupoles is rather tolerable (≈ 15 T/m) but the first (defocusing) final focus quadrupole QD0, providing the vertical beta mm at the IP, is challenging. It should combine the maximum gradient of −32 T/m with extreme compactness to accommodate detector equipment.

Fig. 6 is an artist sketch of the interaction area. It consists of the experimental vacuum vessel with the beams intersecting inside, final focus quadrupoles, vacuum tubes and equipment (pumps, valves, bellows, etc.), beam diagnostics equipment (beam position monitors). The experimental chamber is a flat box with 0.5 mm thick beryllium windows on the box top and bottom to pass $e^\pm$ produced by the dimuonium atoms decay (Fig.6).

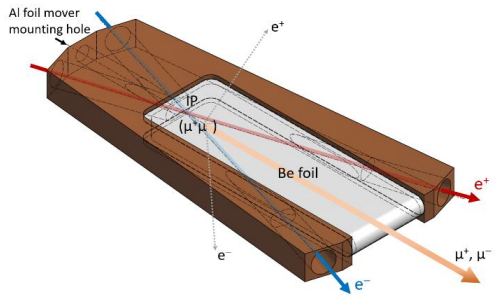


**Fig. 6.** Experimental chamber.

Detector set up for $(\mu^+\mu^-)$ study looks simple and compact; it consists of the tracking systems above and below the median plane, magnetic spectrometer, etc.

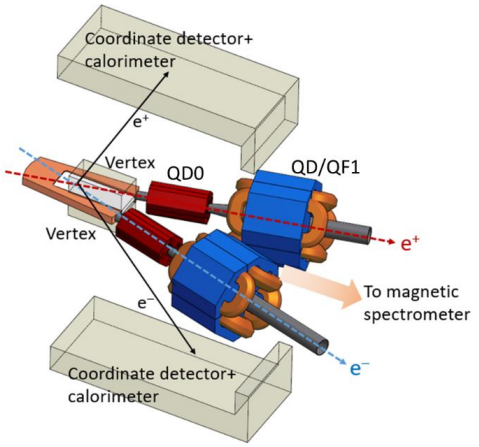


**Fig. 7.** Detector and interaction region equipment.

Four thin-walled stainless steel vacuum tubes with QD0 defocusing quadrupoles over them join the experimental chamber. The quadrupoles are built of permanent magnets and provide the maximum gradient up to − 35 T/m in the Ø30 mm aperture while being very compact and allowing enough room for passing $\mu^+\mu^-$ (or $\pi^+\pi^-$) from the IP toward the magnetic spectrometer. The next quadrupole (QD/QF1 on Fig. 7) is conventional electromagnet and serves either as a focusing (at the low energy) or as an additional defocusing (at the high energy) quadrupole.

Table 2 clearly demonstrates that production rate of dimuonium allows observation of the atom in the reasonable time and investigation of its properties, including spectrum. Fig. 8 illustrates $(\mu^+\mu^-)$ states distribution along the escape line.

**Table 2.** Dimuonium production rate estimation for collider parameters from Table 1.

| ($\mu^+\mu^-$) rate | 1 hour | 4 months |
|---|---|---|
| Totally (1S/2S/3S) | 65/8.1/2.4 | 187k/23k/6.9k |
| For $l$ >2.3 mm | 21/7/2.3 | 59k/20k/6.6k |

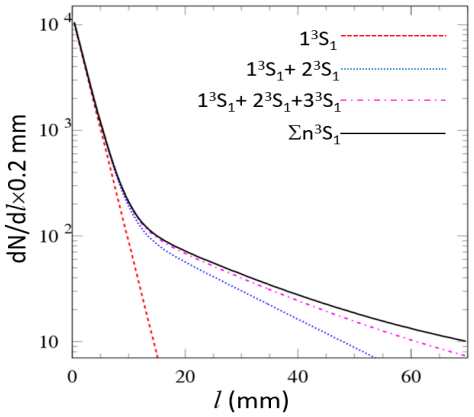


**Fig. 8.** ($\mu^+\mu^-$) distribution along the escape path.

The beam energy 408 MeV under the crossing angle of 70° allows formation of $\pi^+\pi^-$ pairs. The collider parameters are the same as for 75°. To study pions two scenarios are possible: (a) both collision points are modified mechanically from 75° to 70° after the end of the dimuonium research program, (b) simultaneous operation when the beams collide at 75° in the first point to study ($\mu^+\mu^-$) and at 70° in the second point to study $\pi^+\pi^-$.

## 7 Reverse beam configuration

Reverse of one of the beams changes collision angle from 75° to 15° and opens additional possibilities for experiments. In the injection facility energy range (300÷500 MeV) collider with 15° beam crossing allows experiments in the range of $E_{CM} \approx 500 \div 1000$ MeV which includes ρ, ω, η and η′-mesons, etc. Such experiments require a general-purpose detector with solenoid field, which is very much different from the ($\mu^+\mu^-$) detector set up. Thus, the interaction region needs reconfiguration including vacuum chamber, final focus magnets, etc. toward the conventional $e^+e^-$ colliders arrangement. Also, injection polarity in one of the rings should be reversed. As there are no crucial difficulties for that, we do not consider the new configuration in detail and for further estimation apply the lattice from the previous section. We assume adjustment of the new lattice with 15° crossing angle to the optics in Fig.5 and estimate collider parameters by scaling with the energy (considering IBS). Table 3 shows new collider specifications (excluding those repeating the Table 1: circumference, beam current, RF frequency, etc.) for the minimum (η-meson, $m_\eta = 547.8$ MeV, $E_b \approx 284$ MeV) and maximum (η′-meson, $m_{\eta'} = 957.7$ MeV, $E_b \approx 496$ MeV) beam energies.

According to (6) the acute intersection angle significantly increases luminosity. Transverse beam-beam effects although but remain small compared to the head-on collision. The longitudinal beam-beam effects do not change much with respect to 75° collision.

**Table 3.** Collider main parameters for 15° collision angle

| Beam energy (MeV) | 283.59 (η) | 495.78 (η′) |
|---|---|---|
| Invariant mass (MeV) | 547.86 | 957.76 |
| Energy loss per turn (keV) | 0.535 | 4.997 |
| RF voltage (kV) | 300 | 550 |
| Synchrotron tune | $1.67\times10^{-2}$ | $1.71\times10^{-2}$ |
| Horizontal emittance (without/with IBS) (nm) | 11.4/105 | 34.8/75 |
| Energy spread (without/with IBS), $\times10^4$ | 2.8/10.6 | 4.8/8.4 |
| Bunch length (without/with IBS) (mm) | 3.7/14.2 | 6.3/11 |
| IP horizontal angular spread $\sigma_{x'} \times 10^4$ | 8.3 | 7.1 |
| Invariant mass resolution (keV) | 420 | 580 |
| Hor/vert beam-beam parameter ($\xi_x/\xi_y$) | $3\times10^{-4}$ / $1.4\times10^{-2}$ | $3\times10^{-4}$ / $1.3\times10^{-2}$ |
| Longitudinal beam-beam parameter $\xi_z$ | $-1.8\times10^{-3}$ | $-1.7\times10^{-3}$ |
| Peak luminosity for 1 bunch ($cm^{-2}s^{-1}$) | $3.3\times10^{31}$ | $5.2\times10^{31}$ |
| Peak luminosity for 20 bunches ($cm^{-2}s^{-1}$) | $6.6\times10^{32}$ | $1\times10^{33}$ |

## 8 Conclusion

We have considered preliminary design of the electron-positron collider for production and study of ($\mu^+\mu^-$) bound state and capable to perform other experiments with high luminosity in the center-of-mass energy range $E_{CM} \approx 500 \div 1000$ MeV. Two rings collider with large crossing angle is quite compact, the ring orbit length ~20÷30 m, and not expensive in development and maintenance. Despite many challenging issues still needing investigation (dynamic aperture, collective effects, magnet and vacuum systems design, etc.); the project seems interesting for both fundamental research and collider technologies development.

Collider performance and dimuonium production rate allow not only detection of new leptonic atom for the first time but also study ($\mu^+\mu^-$) properties (including precise measurement of the lifetime, spectroscopic experiments, atoms passing through a thin foil, etc.).

## 9 Acknowledgements

We are grateful to

- Yu.A. Pupkov for his important advice to consider extremely low energy $e^+e^-$ collider,
- N.A. Vinokurov, S.I. Seredniakov, E.P. Solodov for many fruitful discussions and valuable comments,

- E.A. Perevedentsev for introduction to and D.N. Shatilov for simulation of the longitudinal beam-beam effects,
- V.A. Kiselev for estimation of the injection schemes and efficiency,
- P.D. Vobly for preliminary design of the quadrupole with permanent magnets.

## References

1. V.N.Baier and V.S.Synakh, Bimuonium production in electron-positron collisions, SOVIET PHYSICS JETP, 14, N5, 1962, pp.1122-1125.
2. H. Lamm, True muonium: the atom that has it all, arXiv 1509.09306v1, 30 Sep 2016.
3. H. Lamm and R.F. Lebed, True Muonium ($\mu^+\mu^-$) on the Light Front, arXiv hep-ph/1311.3245v3, 12 Nov 2014.
4. L.L. Nemenov. Atomic decays of elementary particles. Yad. Fiz., 15:1047-1050, 1972.
5. J.W. Moffat. Does a Heavy Positronium Atom Exist? Phys. Rev. Lett., 35:1605, 1975.
6. E. Holvik and H.A. Olsen. Creation of Relativistic Fermionium in Collisions of Electrons with Atoms. Phys. Rev., D35:2124, 1987.
7. G.A. Kozlov. On the problem of production of relativistic lepton bound states in the decays of light mesons. Sov. J. Nucl. Phys., 48:167-171, 1988.
8. I.F. Ginzburg, U.D. Jentschura, S.G. Karshenboim et al. Production of bound $\mu^+\mu^-$ systems in relativistic heavy ion collisions. Phys. Rev., C58:3565-3573, 1998.
9. N. Arteaga-Romero, C. Carimalo, and V.G. Serbo. Production of bound triplet $\mu^+\mu^-$ system in collisions of electrons with atoms. Phys. Rev., A62:032501, 2000.
10. S.J. Brodsky and R.F. Lebed. Production of the Smallest QED Atom: True Muonium ($\mu^+\mu^-$). Phys. Rev. Lett., 102:213401, 2009.
11. Y.Chen and P.Zhuang. Dimuonium ($\mu^+\mu^-$) Production in a Quark-Gluon Plasma. 2012.
12. A.Banburski and P.Schuster. The Production and Discovery of True Muonium in Fixed-Target Experiments. Phys. Rev., D86:093007, 2012.
13. S.C. Ellis and J. Bland-Hawthorn. On the possibility of observable signatures of leptonic onium atoms from astrophysical sources. 2015.
14. H. Lamm, True muonium on the light front, PhD Dissertation, Arizona State University, May 2016, 115 pages.
15. A. Bogomyagkov and E. Levichev. Collision monochromatization in $e^+e^-$ colliders, Phys. Rev. Accel. Beams 20, 051001, May 2017.
16. V.P. Druzhinin, private communication, March 2017.
17. J.R.Rees, Longitudinal effects of colliding beam space charge force in electron-positron storage rings with crossing angles. SLAC-PUB-781, July 1970.
18. V.V. Danilov et al. Longitudinal effects in beam-beam interaction for an ultra-high luminosity regime. Workshop on beam radiation interaction, UCLA, May 13-16, 1991, World Scientific, pp.1-10.
19. A. Drago et al. Synchrotron oscillation damping by beam-beam collision in DAΦNE, PRST AB 14, 092803 (2011).
20. D. Shatilov, Beam-beam simulation at large amplitudes and lifetime determination. Part. Accel. 52, p.65, 1996.
21. D.E. Berkaev et al., "VEPP-5 Injection Complex: Two Colliders Operation Experience", in Proc. 8th Int. Part.Acc.Conf. (IPAC'17), Copenhagen, Denmark, May 2017, pp. 2982-2984.
22. P. Raimondi et al. Beam-Beam Issues for Colliding Schemes with Large Piwinski Angle and Crabbed Waist, LNF-07/003 (IR) 2007.
23. M. Hosaka et al., Nucl.Instr.Meth. A407 (1998) 234-240.
24. M. Zobov et al., DAΦNE experience with negative momentum compaction, Proc.of EPAC 2006, Edinburgh, Scotland, 989-991.
25. D. Einfeld et al. Design of a Diffraction Limited Light Source (DIFL), in Proc of PAC'95, Dallas, USA (1996)